Optics and Lasers in Engineering 181 (2024) 108387

Contents lists available at ScienceDirect

Optics and Lasers in Engineering

journal homepage: www.elsevier.com/locate/optlaseng

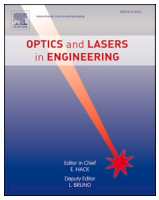

Lossy mode resonance in photonic integrated circuits

Edvins Letko [a,b,*], Arturs Bundulis [a], Edgars Vanags [a], Gatis Mozolevskis [a]

[a] Institute of Solid State Physics, University of Latvia, Riga, LV-1063, Latvia
[b] Faculty of Natural Sciences and Technology, Riga Technical University, Riga, LV-1063, Latvia

ARTICLE INFO

Keywords:
Lossy mode resonance
Photonic integrated circuits
Polymer waveguides
Indium tin oxide
Finite element method

ABSTRACT

In recent years, the promising phenomenon known as lossy mode resonance (LMR) has garnered significant attention in sensing applications. While existing literature in the field of LMR focuses on optical fiber systems and planar waveguides due to their simplicity, there is an absence of research on systems based on photonic integrated circuits (PICs). This article aims to demonstrate, for the first time, the generation of LMR in PICs with sensitivity and a figure of merit (FOM) comparable to that of optical fibers and planar waveguides. Additionally, the article offers a comparison of various polymer materials such as OrmoClear, OrmoCore and SU-8 for integrated waveguides fabrication. To summarize, the main novelty of the article is the demonstration of the LMR phenomenon in integrated chips and the comparison of different polymers commonly used in photonics to fabricate these chips. Moreover, the authors present a novel fabrication workflow for thick polymer waveguides. Finally, the study compares the experimental results obtained with simulations conducted using the finite element method (FEM) in COMSOL Multiphysics environment.

1. Introduction

In recent decades, there has been a growing demand for sensors that utilize optical resonance structures like microcavity-based resonators [1], photonic crystals [2], and plasmonic-based resonators [3], primarily due to their high sensitivity to external influences. A particular attention has been drawn to a phenomenon known as lossy mode resonance (LMR). LMR manifests when light propagates through an optical fiber or waveguide and interacts with a thin film cladding that exhibits a positive real part of permittivity exceeding both its own imaginary part and the permittivity of the light guiding media. When an LMR coating is applied to optical fibers or waveguides, it leads to the creation of attenuation bands in the transmission spectra, which can be attributed to the interaction between the core and lossy modes of the dielectric-cladding film [4]. These attenuation bands exhibit sensitivity to various external factors such as temperature [5], pH [6], humidity [7], concentrations of volatile organic compounds [8], and diverse biomolecules [4], making them highly suitable for numerous sensor applications [4].

LMR offers several advantages over other fiber and waveguide-based sensing techniques. From a design perspective, surface plasmon resonance (SPR) is the technique most similar to LMR. As a result, these methods are typically compared to each other. In certain specific configurations, it is even feasible to generate both phenomena simultaneously [9]. One of the main differences between SPR and LMR phenomena lies in their polarization dependency. Both transverse magnetic (TM) and transverse electric (TE) polarizations can generate LMR, unlike SPR, which is restricted specifically to TM polarization [10]. Furthermore, LMR exhibits the capability to produce multiple resonances [11] and demonstrates greater versatility, being observable with various cladding materials such as polymers [6], semiconductors [12], and dielectrics [13]. This flexibility enhances cost-effectiveness in the manufacturing of sensing devices.

As of today, two primary configurations persist for LMR devices: those utilizing optical fibers [4] and those employing planar waveguides [11]. Initially, LMR was shown in optical fiber setups, benefiting from the ability of multimode fibers to effectively transmit the entire visible and IR spectrum with minimal losses, enabling seamless light propagation between the source, fiber, and spectrometer [4]. Several years ago, the LMR phenomenon was first demonstrated in planar waveguides, offering several advantages. Firstly, planar waveguides provide a more robust platform compared to optical fibers, eliminating the need for splices and simplifying setup handling. Another notable advantage of planar waveguides is their ability to operate across a wide spectrum using either the TE or TM resonance independently. Additionally, planar waveguides allow for thin films to be deposited on both sides, enabling

* Corresponding author at: Institute of Solid State Physics, University of Latvia, Riga, LV-1063, Latvia.
E-mail address: edvins.letko@cfi.lu.lv (E. Letko).

https://doi.org/10.1016/j.optlaseng.2024.108387
Received 24 April 2024; Received in revised form 17 May 2024; Accepted 9 June 2024
Available online 13 June 2024

the development of a two-parameter sensor [11]. Despite all the above advantages of fiber optic and planar waveguide systems, their potential has been nearly maximized, since they do not allow the device to be integrated with other photonic elements on a single chip, a direction toward which the optics and photonics industry is steadily progressing. The transition from the mentioned configurations to integrated photonic circuits is not only logical but also holds great promise. However, successful implementation in this direction has yet to be achieved. This transition poses significant challenges for the fabrication of LMR devices, particularly concerning the requirement for integrated waveguides to transmit the entire visible spectrum simultaneously. This constraint imposes limitations on the minimum size of the waveguide for LMR sensor, thus further necessitate the development of novel fabrication methods for thick waveguides and the materials themselves. Our theoretical research into the LMR phenomenon in integrated waveguides [14] indicates that waveguides with dimensions on the order of tens of micrometers are necessary to observe this effect. Notably, the challenge lies in efficiently coupling light across the entire visible spectrum into the waveguide and collecting the emerging light from the chip. Despite the fabrication and operational challenges associated with LMR devices based on integrated waveguides, this approach offers a distinct advantage - the potential for integration with other photonic elements. For instance, existing literature has demonstrated the feasibility of fabricating an integrated spectrometer [15]. Additionally, successful advancements are being made in the field of on-chip integrated light sources [16]. In the future, this could be integrated on a single chip with an LMR device, marking a significant breakthrough in terms of commercial application. Since the spectrometer and light source typically constitute the most expensive components of a measurement setup, such integration can lead to significant cost savings and increase the practicality of LMR-based devices for a various applications. Furthermore, the shift of LMR sensor technology to PICs is anticipated to garner considerable attention from the industry due to its potential for scalability. This holds particular importance for Point-of-Care (POC) applications and Lab-on-Chip development, where integrated sensors serve as key components [14].

Recently, polymers have risen as promising materials for waveguides fabrication [17]. Unlike their inorganic counterparts, polymers provide cost-effectiveness, flexibility, and the potential for functionalization to attain specific properties tailored for various photonic applications [18]. Among the commercially available polymer materials extensively utilized in integrated photonic applications and amenable to lithographic patterning, negative photoresist SU-8 and the Ormo series of inorganic-organic hybrid polymers are particularly sought after. SU-8 photoresist is prominently used in integrated photonics due to its chemical stability and its ease of patterning through photolithography. Its high transparency makes SU-8 an optimal selection for waveguide applications, particularly in the visible and near-infrared ranges, where LMR is predominantly observable [19]. Integrated SU-8 waveguides find applications in various areas such as microdisk resonators [20], photonic crystals [21], surface plasmon resonance [22], Mach-Zehnder interferometers [23], and more. The Ormo series of photoresists, on the other hand, consists of negative photoresists that come in solvent-free, UV-curable formulations ready for immediate use. They are compatible with UV lithography or UV molding processes. OrmoCore photoresist is known for its low optical losses at data communication wavelengths, high-resolution capabilities down to sub-50 nm pattern dimensions, and high chemical and physical stability [24]. In contrast, OrmoClear photoresist provides superior transparency in the near UV and visible wavelength range when compared to OrmoCore [25]. Ormo series integrated waveguides are utilized across a spectrum of photonic applications, including Bragg gratings [26], ring resonators [27], and bimodal interferometers [28]. It is noteworthy to highlight the advantages of polymer photonics over waveguides composed of inorganic materials, particularly in the context of LMR. Firstly, as mentioned earlier, the dimensions of waveguides needed to generate LMR extend beyond the typical dimensions of silicon-based waveguides. Consequently, fabricating inorganic waveguides with similar dimensions would either be prohibitively expensive or technically infeasible. Moreover, the refractive index of inorganic waveguides tends to be significantly higher than that of polymers. This is crucial, as the sensitivity decreases proportionally with the increasing refractive index of the waveguide [29]. Finally, the increased refractive index of the waveguide prohibits the use of substantial amounts of lossy coating materials.

Table 1
Polymer waveguides photolithography parameters.

Process step	Polymer	Parameters
Spin coating	OrmoClear	2200 rpm for 45 s
	OrmoCore	800 rpm for 45 s
	SU-8	900 rpm for 45 s
Soft bake	OrmoClear	80 °C for 3 min
	OrmoCore	80 °C for 3 min
	SU-8	95 °C for 30 min
Exposure	OrmoClear	i-line filter, 500 mJ/cm^2
	OrmoCore	i-line filter, 500 mJ/cm^2
	SU-8	i-line filter, 300 mJ/cm^2
Post bake	OrmoClear	130 °C for 5 min
	OrmoCore	130 °C for 5 min
	SU-8	95 °C for 10 min
Development	OrmoClear	3 min in OrmoDev
	OrmoCore	3 min in OrmoDev
	SU-8	3 min in mr-Dev 600
Hard bake	OrmoClear	150 °C for 3 h
	OrmoCore	150 °C for 3 h
	SU-8	185 °C for 2 h

This article aims to present a novel integrated LMR device onto a chip, marking a substantial progression not only within the LMR field but also in the broader realm of integrated photonics. Additionally, the study evaluates various polymers for producing integrated waveguides tailored for LMR applications and introduces their innovative fabrication method. Moreover, this research will compare experimental findings with simulations conducted using the finite element method (FEM) in COMSOL Multiphysics, emphasizing the importance of combining experimental data with theoretical analysis, especially considering the novelty of the LMR topic.

2. Materials and methods

Initially, 4″ glass wafers with a thickness of 1.1 μm underwent wet cleaning using detergent, acetone, and isopropanol in an ultrasonic bath operating at 37 kHz frequency for 10 min for each solvent. Subsequently, the cleaned wafers were subjected to oxygen plasma ashing in a GIGAbatch 360 M tool at 800 W and 1000 sccm of O_2 flow for 10 min. Following this, a 100 nm thick aluminum layer was thermally evaporated onto the wafers. To enhance the adhesion of the AZ1518 photoresist, HMDS priming was applied to the aluminum surface, followed by spin coating of the photoresist at a speed of 4000 rpm for 30 seconds using Laurell WS650 spin coater. A soft bake at 100 °C for 2 min was then conducted. The next step involved selective direct laser exposure with a dose of 60 mJ/cm^2 using a μPG Heidelberg laser writer, resulting in the pattern of future polymer waveguides. After exposure, the AZ1518 photoresist was developed in AZ 726 MIF developer for 1 minute. Subsequently, samples with AZ1518 structures underwent a hard bake at 130 °C for 10 min. Following the hard bake of AZ1518, wet etching of the aluminum was performed in AZ 726 MIF at 70 °C for 1 minute. These etched aluminum structures will serve as photolithography mask on the wafer itself. The next step involved stripping the photoresist in acetone for 1 minute. At this stage, the wafers consisted only of aluminum structures and were ready for the polymer waveguide fabrication sequence. Oxygen plasma ashing was conducted once more prior to the photolithography procedure. For each wafer, specific polymer (OrmoClear, OrmoCore, and SU-8) underwent spin coating, soft bake,

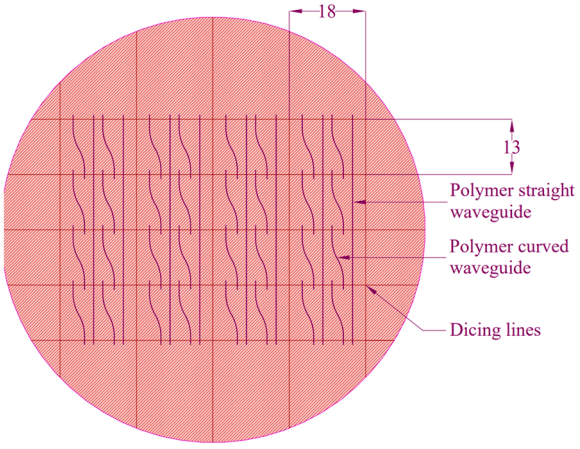

Fig. 1. Schematic top view of the fabricated wafer with polymer waveguide structures.

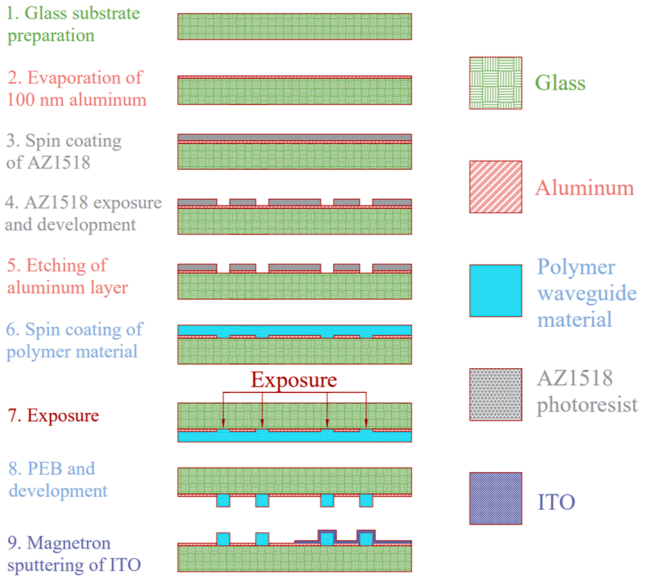

Fig. 2. LMR chip fabrication workflow.

exposure, post bake, development, and hard bake steps, with specific parameters indicated in the accompanying Table 1. A notable aspect of this photolithography procedure was the exposure step, where exposure was conducted using the Mask Aligner Suss MA6 tool from the bottom of the substrate - exposure was carried out through the glass substrate and etched aluminum openings. This approach proved advantageous for several reasons. Firstly, Ormo series photoresists are solvent-free and remain liquid even after the soft bake, making only proximity exposure possible. Secondly, the standard photolithography masking approach would result in a pronounced trapezoid shape of the waveguide cross-section for thick structures, whereas exposure from the bottom resulted in a slightly negative trapezoid shape. This negative trapezoid shape compensates the temperature gradient during the post bake and the slightly different development rates on the waveguide top and bottom, resulting in a more rectangular cross-section compared to standard proximity exposure. As a result, three wafers were produced, each containing waveguide structures made of OrmoClear, OrmoCore, and SU-8, respectively. The next stage involved outsourcing the wafer saw dicing services to DISCO HI-TEC EUROPE GmbH to divide each wafer into 16 chips measuring 13 × 18 mm. A schematic representation showing the fabricated wafer with polymer structures and the saw

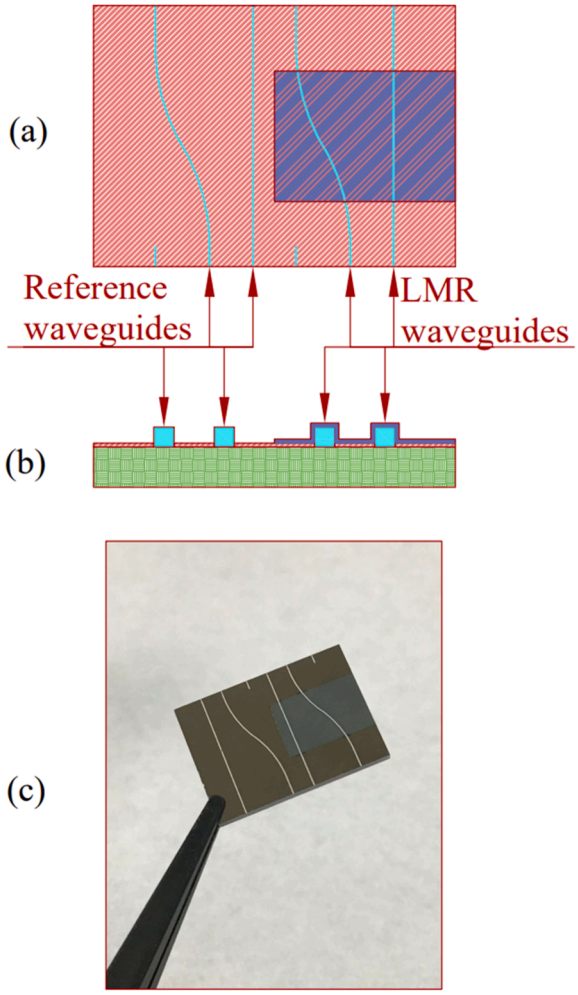

Fig. 3. The final design of the LMR chip: (a) top view, (b) cross-sectional view, (c) a photo of the actual device.

dicing pattern is provided in the Fig. 1. Each chip on the wafer contains both straight and curved waveguides to explore the dependency of the LMR phenomenon on waveguide geometry.

Our recent research [30] about LMR in planar waveguides highlighted indium tin oxide (ITO) as the most suitable material among the commonly used options due to its ability to produce profound LMRs across the entire visible spectrum. Consequently, for our integrated LMR chips, we opted for ITO as the lossy coating. Upon receipt of the diced wafer, the deposition of ITO coating over each fabricated chip was performed using the Sidrabe G500M DC magnetron sputtering system. The ITO coating process utilized an ITO (In_2O/SnO_2 with a weight ratio of 9:1) target measuring 100 × 200 × 9 mm, at a pressure of 5 mTorr and a power of 200 W using Ar plasma. To enable selective area deposition, the chip was masked with Kapton tape, facilitating the provision of both reference and LMR waveguides on the same sample. Fig. 2 illustrates the entire fabrication workflow of the LMR chip. This fabrication process yields the device depicted in Fig. 3.

Spectral ellipsometry was employed using the Woollam RC2-XL instrument and CompleteEASE software manual to assess the optical properties of the deposited ITO coating. Moreover, ellipsometry analysis was conducted to ascertain the thickness of the ITO coating over the waveguides following each deposition procedure. Measurements were conducted across the visible and near-infrared regions, covering angles of incidence ranging from 50° to 70°. This data was subsequently used to fit Lorentz oscillator [31] parameters, facilitating the calculation of the dielectric permittivity of ITO [32]:

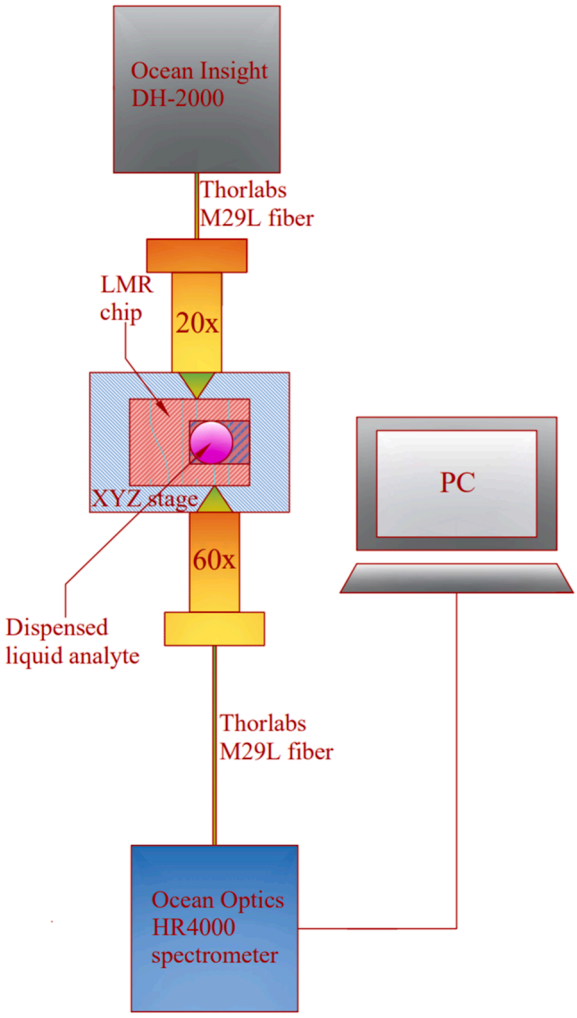

Fig. 4. Experimental setup.

$$\varepsilon = \varepsilon_\infty + \frac{Amp}{En^2 - E^2} + \sum \frac{Amp_n Br_n En_n}{En_n^2 - E^2 - iEBr_n}, \tag{1}$$

where all parameters except E are fitted parameters. The dispersion characteristics of the glass substrate were determined utilizing the Sellmeier equation [33] from CompleteEASE:

$$n = \sqrt{\varepsilon_\infty + \frac{A\lambda^2}{\lambda^2 - B^2} - E\lambda^2}\,, \tag{2}$$

where λ denotes the wavelength in micrometers, while A, B and E are coefficients derived through fitting. Highly precise optical properties of polymers are furnished by photoresist manufacturers ($n_{\mathrm{Ormo}} = 1.5414 + 0.0019/\lambda^2 + 0.0013/\lambda^4$ and $n_{\mathrm{SU-8}} = 1.5690 + 0.0088/\lambda^2 + 0.0004/\lambda^4$ for Ormo series [34] and SU-8 [35], respectively), yet information regarding the optical properties of the glass substrate and ITO was unavailable. Consequently, ellipsometry was exclusively employed for analyzing the ITO coating and glass substrate.

The Thermo Scientific™ Helios™ 5 UX high-resolution field emission scanning electron microscope (SEM) was employed to examine the cross-section of the waveguide and evaluate the homogeneity of the deposited lossy coating. Imaging procedures were carried out using an electron acceleration voltage of 2 kV and a beam current of 25 pA, with secondary electrons detected using both a through-the-lens detector (TLD) and an ion conversion and electron (ICE) detector. To counteract charging effects during imaging, scan interlacing and integration

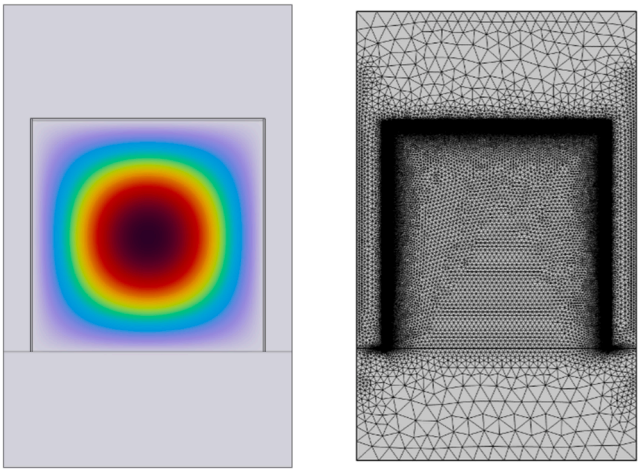

(a) (b)

Fig. 5. 2D cross-section geometry in COMSOL simulation: (a) example of electromagnetic field distribution in a polymer waveguide, and (b) user-controlled mesh.

methods were applied. To explore the waveguide cross-section within the region of the lossy coating via SEM analysis, samples were initially scribed from the underside of the substrate using a diamond scriber RV-129 and then fractured using a cleaving tool. Although this method poses the risk of causing localized damage to the polymer waveguides and introducing contamination, it was deemed appropriate for the cross-sectional analysis of the devices.

To characterize the LMR spectrum of the produced devices, a custom-built experimental setup was utilized. Light emanating from an Ocean Insight DH-2000 source was directed through an optical fiber (Thorlabs M29L) and then coupled into the sample. The resulting signal was collected via an optical fiber and analyzed using the Ocean Optics HR4000 spectrometer. Measurements were conducted for both the fabricated devices and planar waveguides to compare the behavior of the PICs with a well-established configuration. In the case of planar waveguides, light was directly coupled from the fiber into the glass substrate from the side, and the outgoing light was similarly collected through the fiber. This method has previously proven effective in our previous work on LMR in planar waveguides [30]. Typically, LMR measurement setups include polarizers to separate TE and TM modes. However, for this study, it was decided not to employ such optical elements to avoid signal reduction, which is crucial for integrated waveguides. In the case of devices based on waveguides, the light was focused onto the waveguide facet using a 20x microscope objective, and the output light was subsequently coupled back into the fiber using a 60x microscope objective (refer to Fig. 4). The LMR chip was positioned on XYZ stage to ensure precise light coupling.

The performance of the designed device was simulated using COMSOL Multiphysics. Initially, a two-dimensional cross-sectional geometry was established to analyze the electromagnetic distribution of guided modes within 100 × 100 μm polymer waveguides (refer to Fig. 5a). Following this, various materials were defined, including glass substrate, ITO, SU-8, OrmoClear, OrmoCore, and the sensing mediums. The optical properties of ITO and the glass substrate were established via spectral ellipsometry, whereas the optical properties of the other materials were sourced from provided data sheets. The "Electromagnetic Waves, Frequency Domain" physics module was employed to address the defined issues. Meshing of the geometry was performed with user-controlled element sizes: the lossy coating domain, being the most tiny structure, was meshed with element sizes less than 50 nm; the waveguide domain was meshed with element sizes less than 1 μm, and the remaining domains were meshed with element sizes less than 10 μm.

Table 2
Materials fitted parameters.

Material	Fitted parameters
ITO	$\varepsilon_\infty = 2.32$, $Amp = 71.43\ eV^2$, $En = 7.33\ eV$, $Amp_1 = 3.71$, $Br_1 = 0.37\ eV$, $En_1 = 3.86\ eV$, $Amp_2 = 40.57$, $Br_2 = 0.06\ eV$, $En_2 = 0.52\ eV$.
Glass	$\varepsilon_\infty = 1.00$, $A = 1.17$, $B = 0.09\ \mu m^2$, $E = 0.01\ \mu m^{-2}$.

The mesh comprised 260,000 triangular elements and 10,000 edge elements, covering an area of $2{\cdot}10^{-8}$ m^2, with the majority of elements situated in the thin film structure (refer to Fig. 5b). A parametric sweep was conducted to explore various coating thicknesses and materials. Calculations were performed within a spectral range from 500 nm to 900 nm due to poor transmittance outside this range for polymer structures.

Mode analysis was conducted to examine the distribution of the electromagnetic field in the polymer waveguide, facilitating the assessment of the effective refractive index n_{eff}. This parameter was subsequently utilized to simulate transmittance spectra using equation [36]:

$$T = \exp\left(-\frac{4\pi}{\lambda}\,\text{imag}(n_{\text{eff}})L\right), \tag{3}$$

where T represents transmittance, λ stands for wavelength, and L represents the length of the sensing region, which is 1 cm.

3. Results and discussion

The optical properties acquired through spectral ellipsometry, which were subsequently utilized in simulations, are presented in the Table 2.

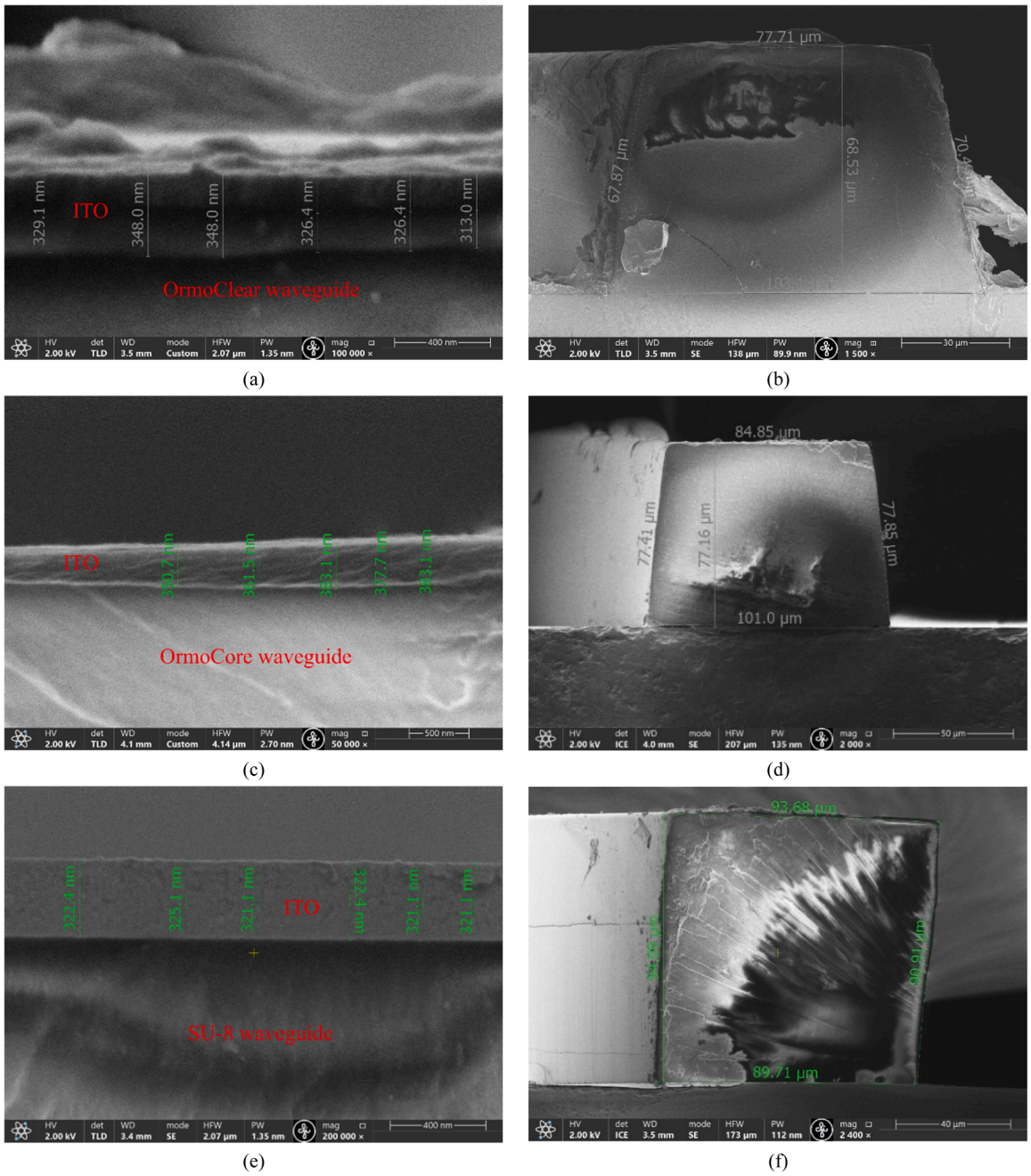

Fig. 6. SEM analysis: (a) ITO on an OrmoClear waveguide, (b) cross-section of an OrmoClear waveguide, (c) ITO on an OrmoCore waveguide, (d) cross-section of an OrmoCore waveguide, (e) ITO on a SU-8 waveguide, and (f) cross-section of a SU-8 waveguide.

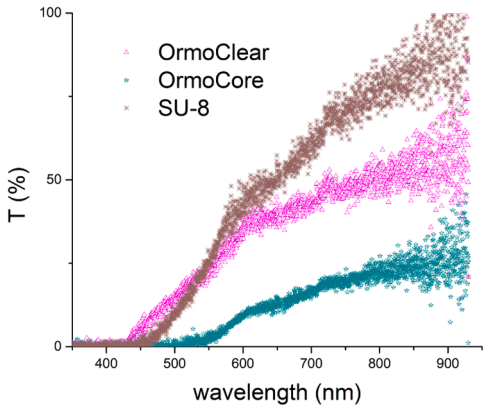

Fig. 7. Different polymer waveguide transmittance performance.

Scanning electron microscopy revealed that the cross-sectional shape of the waveguides closely resembled a square type (refer to Fig. 6), particularly evident in the SU-8 waveguide, thereby validating the success of proposed novel photolithography technique in fabricating thick waveguides. For OrmoClear and OrmoCore waveguides, the cross-sectional shape still retains a slight trapezoidal form, likely attributable to the liquid state of the photoresist following the soft bake process. Analysis of SEM images indicates slight dimensional variations among the OrmoClear, OrmoCore, and SU-8 waveguide structures, potentially impacting the output signal power. These dimensional and shape differences may partly account for the observed variations in transmittance power across different polymers. Additionally, SEM was employed to assess the uniformity of the ITO coating. Thickness variations in the ITO coating were approximately 4 % for OrmoClear and OrmoCore waveguides, while for SU-8, it was less than 1 %. As depicted in Fig. 6e, the edge of the SU-8 waveguide appears flatter and smoother compared to OrmoClear and OrmoCore waveguides (refer to Fig. 6a and Fig. 6c, respectively), which may contribute to the more homogeneous thin film growth on the surface of the SU-8 waveguide.

Fig. 7 demonstrates the ability of various polymer waveguides to effectively transmit the entire spectrum of the light source. All acquired spectra were normalized to the spectrum of the light source. It is evident that SU-8 and OrmoClear waveguides exhibit similar transmittance performance over a 100 ms integration time, while the OrmoCore waveguide shows significantly lower performance, as expected given its intended application. OrmoCore waveguides are designed for use in data communication wavelengths, hence higher losses were anticipated. Conversely, OrmoClear waveguides are optimized for efficiency in the visible and near-UV regions, resulting in superior transmission, particularly below 500 nm, even outperforming SU-8 waveguides. However, for wavelengths beyond 500 nm, SU-8 waveguides display slightly better performance. Furthermore, the working wavelength range spans from 500 nm to 900 nm, indicating that all subsequent spectra and theoretical calculations will be precisely conducted within this range. This can be attributed to the high optical losses for wavelengths below 500 nm and the low output light intensity of the source for wavelengths above 900 nm, evident from the significantly higher background noise compared to the rest of the spectrum. In fabricated devices, optical power losses occur from various sources, including light coupling from the optical fiber to the waveguide, scattering and absorption within the polymer waveguide, and bending losses. In the optimal wavelength range around 800 nm, optical power losses are 2.3 dB/cm, 4.6 dB/cm and 1.0 dB/cm for OrmoClear, OrmoCore and SU-8 waveguides, respectively. The wavelength thresholds are 440 nm, 470 nm, and 550 nm for the OrmoClear, SU-8, and OrmoCore waveguides, respectively.

The Fig. 8a provides a comparison of LMRs observed in both straight and curved waveguides for OrmoClear and SU-8 polymers. It is evident that, regardless of the waveguide geometry, the depth of LMR peaks and the full width at half minimum (FWHM) are similar for polymer both waveguides. In essence, the LMR behavior in waveguides with curved geometry does not differ from those with straight geometry, suggesting no requirement for additional testing of both configurations, leading to the decision to focus measurements exclusively on straight waveguides due to their lower optical losses. It is worth noting that comparison data for OrmoCore waveguides are not depicted in Fig. 8a due to their notably lower transmittance and the complexities associated with observing LMRs in curved waveguides. However, LMRs were observable for all explored straight polymer waveguides, including OrmoCore, when utilizing a 540 nm thick ITO coating. The transmittance spectra for these devices are provided in the Fig. 8b. It is worth noting that at an ITO coating thickness of 80 nm, only first-order LMR is observed. It is widely known that in this LMR order the resonance lines for TE and TM polarizations are separated even without the use of a linear polarizer (refer to Fig. 8a) [11]. However, for higher-order LMRs, the resonance lines of TE and TM polarizations become closer to each other with each subsequent order. As a result, observing TE and TM resonances separately

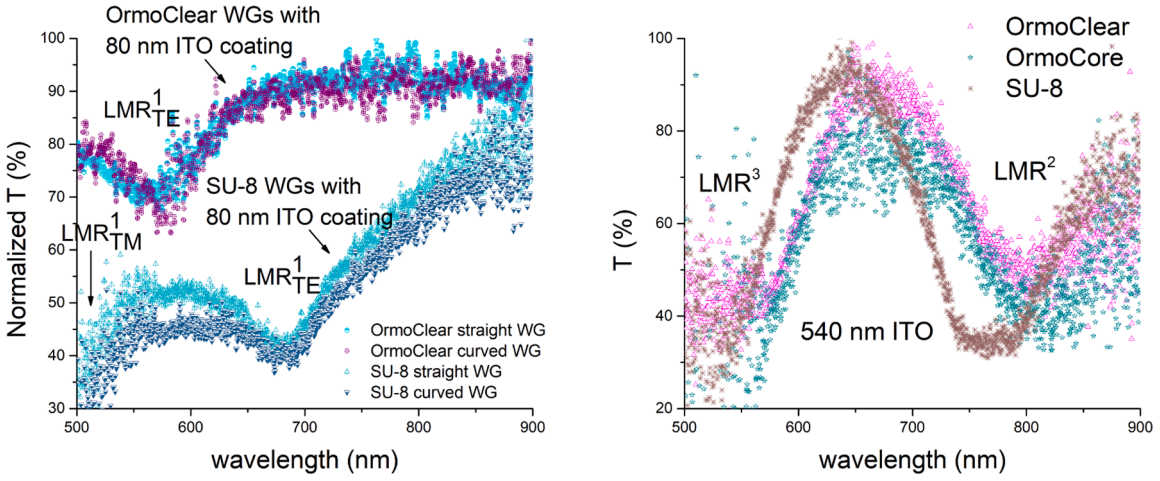

Fig. 8. Comparison of LMR in different types of waveguides: (a) comparison in straight and curved waveguide, and (b) comparison in waveguides of different polymers.

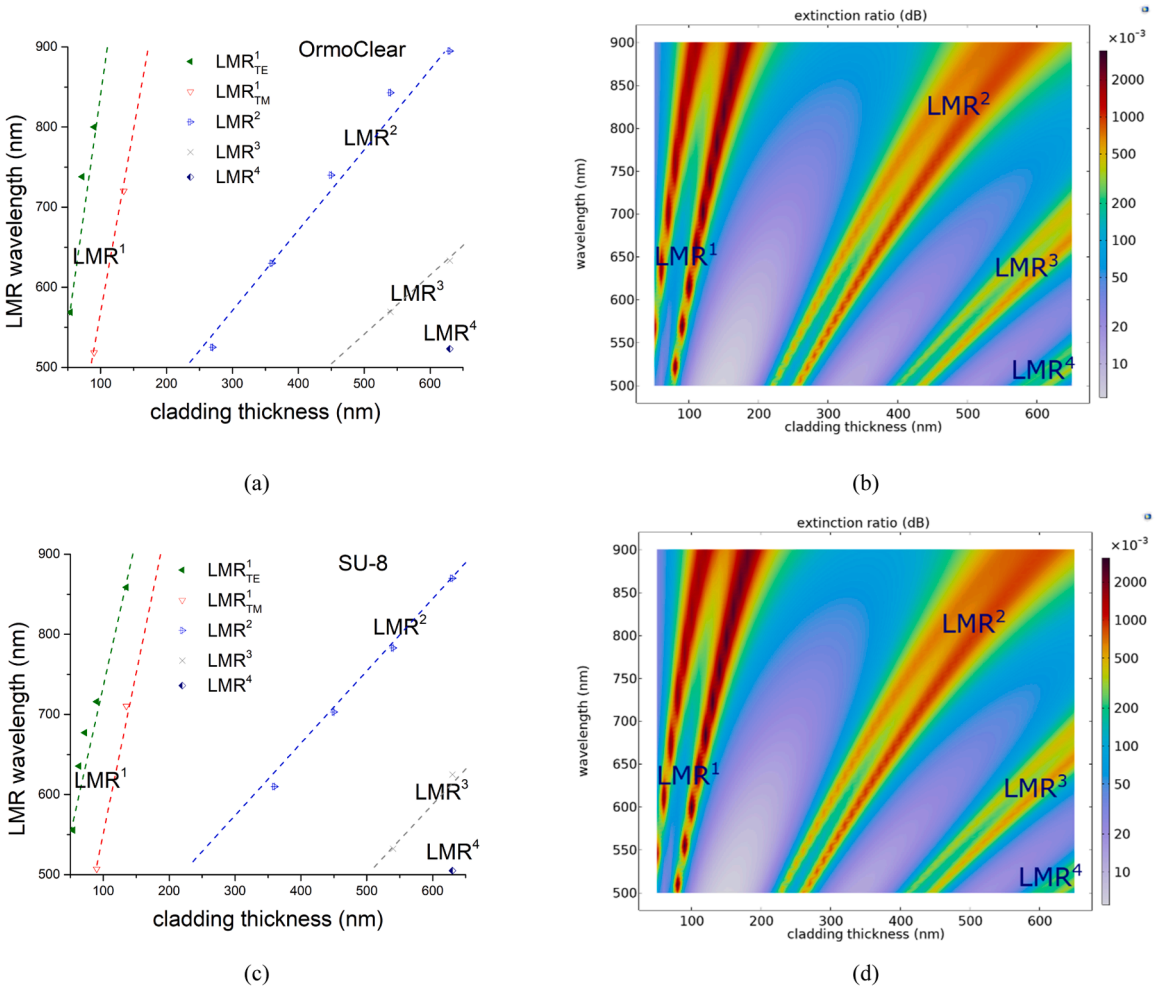

Fig. 9. LMRs in dependence of wavelength and ITO thickness: (a) experimental results for OrmoClear waveguides, (b) theoretical results for OrmoClear waveguides, (c) experimental results for SU-8 waveguides, and (d) theoretical results for SU-8 waveguides.

without using a linear polarizer becomes impossible. Therefore, in Fig. 8b, only the LMR order can be identified, but not the polarization in which the resonance was observed. In addition, Fig. 8 shows that the LMR wavelengths differs slightly between the SU-8 and Ormo series polymers, which is explained by slight differences in their refractive indices. Conversely, LMRs in the OrmoClear and OrmoCore waveguides occur at similar wavelengths, as expected theoretically due to their nearly identical refractive indices (refer to Fig. 8b).

Comparing experimental results with simulations commonly involves utilizing color plots spanning various cladding thicknesses. This method provides a comprehensive assessment of whether the theoretical model effectively matches the physics of the LMR phenomenon in fabricated devices. Theoretical calculations of extinction ratios corresponding to different ITO coating thicknesses are depicted as a function of wavelength in the Fig. 9. Again, for both SU-8 and OrmoClear polymer waveguides, experimentally obtained separated TM and TE polarizations were achieved only for the first-order LMR, whereas for higher-order LMRs, these modes overlap and manifest as a single peak. The experimental setup did not utilize a polarizer to differentiate between different guided modes. Conversely, mode analysis in COMSOL Multiphysics simulates each mode independently, hence theoretically, two resonances were expected for every LMR order. These disparities between theoretical predictions and experimental findings constitute the main differences. The minor deviations of the resonant wavelengths are due to the inhomogeneity and roughness of the ITO coating, which was theoretically demonstrated in our previous study [30]. For OrmoCore waveguides, such dependencies were challenging to ascertain due to the difficulties in observing LMRs for every cladding thickness - most cases encountered critical losses, impeding the generation of LMRs.

For sensitivity assessment, a device utilizing SU-8 waveguides was chosen for its lower optical losses, facilitating the evaluation of sensitivity characteristics. Various liquids were applied to the sensing area to monitor the shift in the LMR. The precise determination of LMR peak shapes and resonance wavelengths proved challenging due to signal noise, particularly in TM polarization (refer to Fig. 10a). Consequently, Gaussian approximations were employed to estimate the acquired spectra, streamlining the analysis process. Fig. 10a and Fig. 10b depict the first-order LMRs for SU-8 waveguides and planar waveguides, respectively. For the first-order LMRs, an 80 nm thick ITO coating was selected because at this thickness, both TE and TM mode resonances are observable within the operational wavelength range of 500 nm to 900 nm when measuring signals in a liquid environment. The sensitivity and FWHM for both configurations exhibit notable similarity, proving competitive performance between integrated waveguides and the well-established planar waveguide design. This trend extends to higher-order LMRs, as observed in Fig. 10c and d. For higher-order LMRs, a 630 nm thick ITO coating was selected because it enables the simultaneous observation of the largest number of LMRs (LMR [2], LMR [3], and LMR [4]) within the operational wavelength range. Thinner coatings allow only LMR [2] and LMR [3] to be observed simultaneously. Given the significantly higher sensitivity for first-order LMRs, sensitivity measurements were conducted using liquids with refractive indices ranging

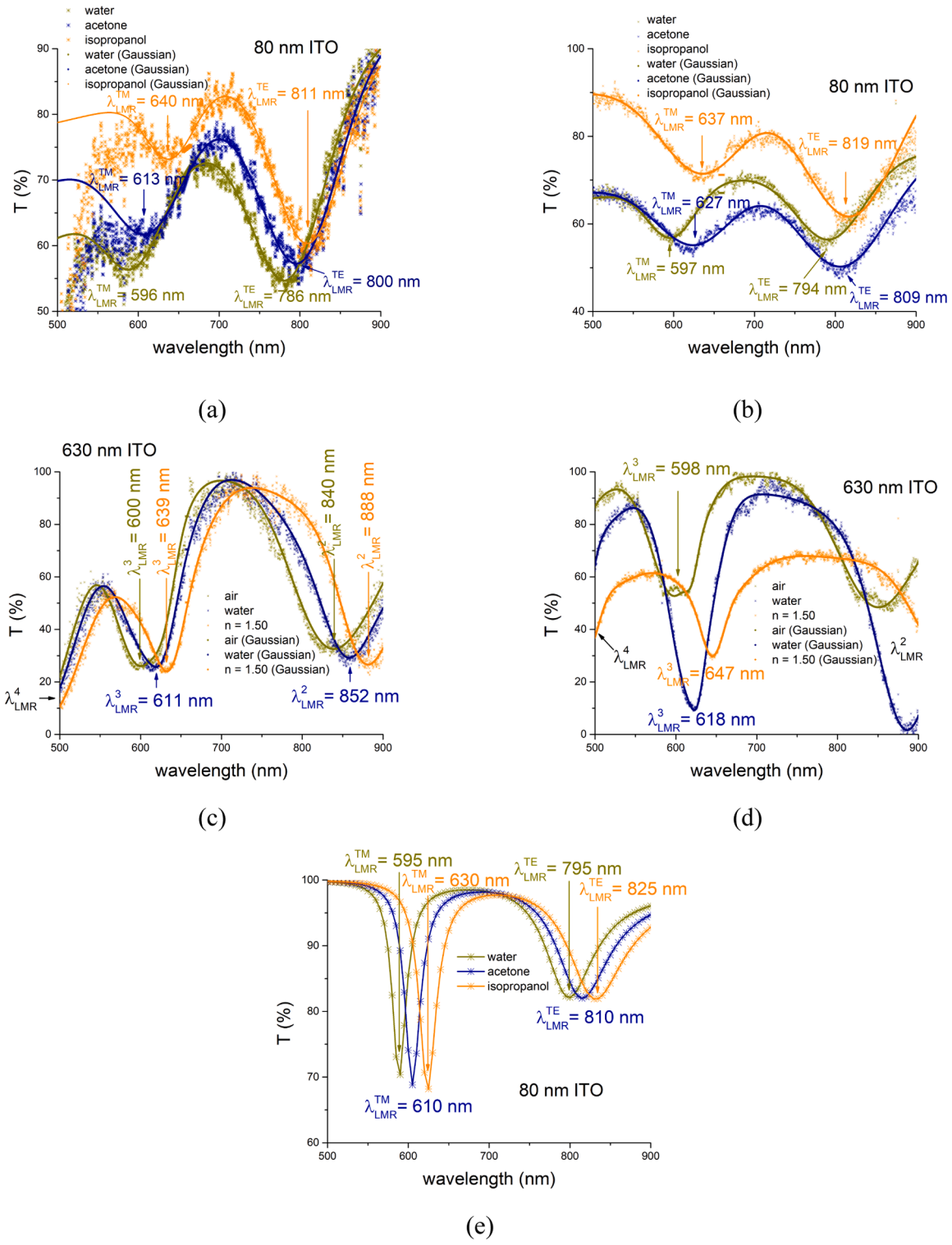

Fig. 10. Experimental sensing response in various liquids: (a) first-order LMRs in an integrated device based on SU-8 waveguides, (b) first-order LMRs in a planar glass waveguide, (c) higher-order LMRs in an integrated device based on SU-8 waveguides, (d) higher-order LMRs in a planar glass waveguide, and (e) theoretically calculated first-order LMRs in an integrated device based on SU-8 waveguides.

from 1.33 to 1.39, while for higher-order LMRs, sensitivity measurements encompassed environments with refractive indices ranging from 1.00 to 1.50. Simulations were also conducted for SU-8 waveguide coated with an 80 nm thick layer of ITO to compare the theoretical performance of the device with the experimental results (refer to Fig. 10e). While slightly different LMR wavelengths and peak shapes were anticipated theoretically compared to those obtained experimentally, these differences were minor. Surprisingly, the observed experimental sensitivity was higher than theoretically expected. This can be explained by small differences in the optical dispersion of the medium specified in the simulation compared to the real data. The first-order LMRs as a function of the refractive index of the medium for both TM and TE polarizations for the SU-8 waveguide and the planar waveguide are shown in the Fig. 11. As evident from the data, the

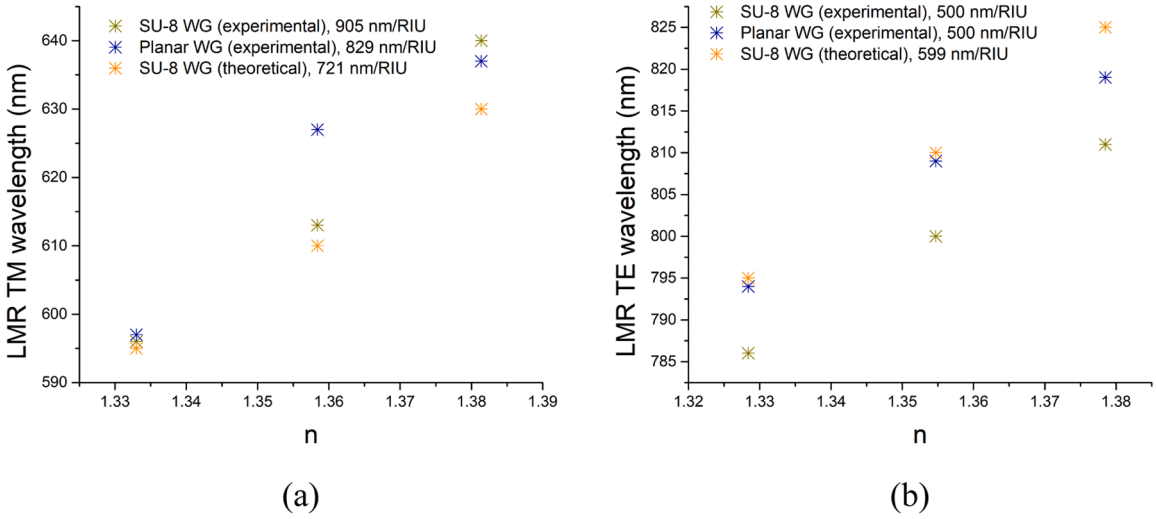

Fig. 11. First-order LMR sensing performance: (a) TM mode, and (b) TE mode.

Table 3
Sensor sensitivities and FOMs.

Analysis	Waveguide type	$S, \frac{\text{nm}}{\text{RIU}}$	FOM, RIU^{-1}
Experimental	SU-8, TM mode	905	23
	SU-8, TE mode	500	10
	Planar, TM mode	829	21
	Planar, TE mode	499	10
Theoretical	SU-8, TM mode	721	25
	SU-8, TE mode	599	12

sensitivity for TM mode considerably surpasses that of TE mode in both theoretical and experimental observations, consistent with expectations outlined in the literature [37].

The primary standardized parameter that characterizes the overall performance of a sensing device is the figure of merit (FOM) [38], defined by the equation:

$$\text{FOM} = \frac{S}{\text{FWHM}}, \tag{4}$$

where S represents the slope of the function $\lambda_{\text{LMR}} = f(n)$. The calculated FOMs and sensitivities for the fabricated device based on SU-8 waveguide, planar waveguide, and theoretically simulated device based on SU-8 waveguide are summarized in the Table 3. Given that first-order LMRs are known for higher sensitivity and FOM, it was decided to focus specifically on this order LMRs and not consider higher-order LMRs. It is evident that the sensitivities and FOMs for both integrated SU-8 waveguides and planar waveguides exhibit remarkable similarity, underscoring the competitiveness and promise of integrated waveguides in the field of LMR. In fact, the TM mode sensitivity achieved in the SU-8 waveguide surpasses that of the planar waveguide by 8 %, with values of 905 nm/RIU compared to 829 nm/RIU. The theoretically calculated and experimentally obtained FOMs for device based on SU-8 have very similar values. The experimental sensitivity in TM mode exceeded the theoretical prediction. However, the experimentally obtained FWHM was broader as a consequence of the thickness variations confirmed in our recent research [30], leading to nearly identical FOM values.

4. Conclusions

This study marks a significant advancement, showcasing the LMR effect for the first time within integrated on-chip hybrid organic-inorganic systems. This achievement represents substantial progress not only in the field of LMR but also in the broader field of photonics. The main novelty of this research is the successful observation of the LMR phenomenon in different types of integrated polymer waveguides covering different materials (OrmoClear, OrmoCore and SU-8) as well as geometries (straight and curved). Among the tested materials, SU-8 emerged as better polymer at guiding the entire visible light spectrum, thereby facilitating more pronounced LMRs compared to other polymer materials. Moreover, it was demonstrated that waveguide geometry has minimal impact on LMR, except for a decrease in light intensity observed in curved waveguides due to bend losses.

With the exception of OrmoCore, every tested polymer material exhibited LMR dependence on cladding thickness and resonance wavelength consistent with predictions from theoretical simulations conducted via COMSOL Multiphysics. The primary differences arose from the measurement setup, which did not employ a linear polarizer. Consequently, it was not feasible to observe TM and TE modes separately for higher-order LMRs, as predicted by theoretical calculations. Additionally, experimentally obtained FOM closely aligned with simulated predictions.

This article introduces a novel fabrication method for thick waveguides, involving exposure through the glass substrate and aluminum mask positioned directly on the chip. This technique yields waveguides with a more rectangular cross-sectional profile, and in the case of SU-8 waveguides, it even resulted in a slightly negative trapezoidal shape. This approach enables the production of high-quality waveguides capable of propagating light to observe LMR, a capability not achievable with other fabrication techniques.

The FOM and sensitivity performance of integrated polymer-based devices and planar waveguides showed similarity for both setups, highlighting the promising potential of integrated systems in the LMR field. Integrated waveguides, in contrast to planar counterparts, exhibit enhanced flexibility, indicating that continued development in this direction could position them as dominant alternatives to planar waveguides and fiber-based configurations.

A key advantage of photonic integrated circuits lies in their ability to integrate diverse elements on a single chip to deliver unique functionalities. The next stage in the development of integrated LMR sensors could involve integrating them with spectrometers and on-chip light sources, thereby significantly reducing device costs.

Author agreement statement

We the undersigned declare that this manuscript is original, has not been published before and is not currently being considered for

publication elsewhere.

We confirm that the manuscript has been read and approved by all named authors and that there are no other persons who satisfied the criteria for authorship but are not listed. We further confirm that the order of authors listed in the manuscript has been approved by all of us.

We understand that the Corresponding Author is the sole contact for the Editorial process. He/she is responsible for communicating with the other authors about progress, submissions of revisions and final approval of proofs

CRediT authorship contribution statement

Edvins Letko: Writing – original draft, Methodology, Investigation, Formal analysis, Conceptualization. **Arturs Bundulis:** Writing – review & editing, Methodology. **Edgars Vanags:** Visualization. **Gatis Mozolevskis:** Writing – review & editing, Supervision.

Declaration of competing interest

The authors declare the following financial interests/personal relationships which may be considered as potential competing interests: Edvins Letko reports financial support and article publishing charges were provided by University of Latvia Institute of Solid State Physics. If there are other authors, they declare that they have no known competing financial interests or personal relationships that could have appeared to influence the work reported in this paper.

Data availability

Data will be made available on request.

Acknowledgment

The authors would like to acknowledge the Institute of Solid State Physics, University of Latvia. This research was supported by the European Regional Development Fund project 1.1.1.1/20/A/045 and the European Union's Horizon 2020 Framework Program H2020-WIDESPREAD-01-2016-2017-TeamingPhase2 under grant agreement No. 739508, project CAMART2. This work was supported by National Research Program 'Smart Materials, Photonics, Technologies and Engineering Ecosystem' (project No. VPPEM-FOTONIKA-2022/1-0001).

References

[1] Ali L, Mohammed MU, Khan M, Yousuf AHB, Chowdhury MH. High-quality optical ring resonator based biosensor for cancer detection. IEEE Sens J 2019;1(C): 1867–75. https://doi.org/10.1109/JSEN.2019.2950664. *PP*.

[2] Inan H, Poyraz M, Inci F, Lifson MA, Baday M, Cunningham BT, Demirci U. Promise for point-of-care applications. Chem Soc Rev 2016:366–88. https://doi.org/10.1039/C6CS00206D.

[3] Ramirez JC, Grajales García D, Maldonado J. Fernández-Gavela, A. Current trends in photonic biosensors: advances towards multiplexed integration. Chemosensors 2022;10(10):398–420. https://doi.org/10.3390/chemosensors10100398.

[4] Wang Q, Zhao WM. A comprehensive review of lossy mode resonance-based fiber optic sensors. Opt Lasers Eng 2018;100(July 2017):47–60. https://doi.org/10.1016/j.optlaseng.2017.07.009.

[5] Sánchez P, Zamarreño CR, Arregui FJ, Matías IR. LMR-based optical fiber refractometers for oil degradation sensing applications in synthetic lubricant oils. J Light Technol 2016;34(19):4537–42. https://doi.org/10.1109/JLT.2016.2562701.

[6] Zamarreño CR, Hernáez M, Del Villar I, Matías IR, Arregui FJ. Optical fiber PH sensor based on lossy-mode resonances by means of thin polymeric coatings. Sens Actuators, B Chem 2011;155(1):290–7. https://doi.org/10.1016/j.snb.2010.12.037.

[7] Zamarreño CR, Hernaez M, Del Villar I, Matias IR, Arregui FJ. Tunable Humidity sensor based on ITO-coated optical fiber. Sens Actuators, B Chem. 2010;146(1): 414–7. https://doi.org/10.1016/j.snb.2010.02.029.

[8] Elosúa C, Vidondo I, Arregui FJ, Bariain C, Luquin A, Laguna M, Matías IR. Lossy mode resonance optical fiber sensor to detect organic vapors. Sens Actuators, B Chem 2013;187:65–71. https://doi.org/10.1016/j.snb.2012.09.046.

[9] Del Villar I, Zamarreño CR, Hernaez M, Arregui FJ, Matias IR. Lossy mode resonance generation with indium-tin-oxide-coated optical fibers for sensing applications. J Light Technol 2010;28(1):111–7. https://doi.org/10.1109/JLT.2009.2036580.

[10] Fuentes O, Goicoechea J, Corres JM, Villar IDel, Ozcariz A, Matias IR. Generation of lossy mode resonances with different nanocoatings deposited on coverslips. Opt Express 2020;28(1):288–301. https://doi.org/10.1364/oe.28.000288.

[11] Fuentes O, Del Villar I, Corres JM, Matias IR. Lossy mode resonance sensors based on lateral light incidence in nanocoated planar waveguides. Sci Rep 2019;9(1): 1–10. https://doi.org/10.1038/s41598-019-45285-x.

[12] Arregui FJ, Villar IDel, Corres JM, Goicoechea J, Carlos R, Elosua C, Hernaez M, Rivero PJ, Socorro AB, Sanchez P, Zubiate P, Lopez D, Acha NDe. Matias, I. R. Fiber-optic lossy mode resonance sensors. Procedia Eng 2014;87:3–8. https://doi.org/10.1016/j.proeng.2014.11.253.

[13] Refractometer, F.; Sudas, D. P.; Zakharov, L. Y.; Jitov, V. A.; Golant, K. M. Silicon oxynitride thin film coating to lossy mode resonance. 2022, 1–12.

[14] Letko E, Bundulis A, Mozolevskis G. Theoretical development of polymer-based integrated lossy-mode resonance sensor for photonic integrated circuits. Photonics 2022;9(10):764–73. https://doi.org/10.3390/photonics9100764.

[15] Li A, Yao C, Xia J, Wang H, Cheng Q, Penty R, Fainman Y, Pan S. Advances in cost-effective integrated spectrometers. Light Sci Appl 2022;11(1):1–18. https://doi.org/10.1038/s41377-022-00853-1.

[16] Zhou Z, Yin B, Michel J. On-Chip light sources for silicon photonics. Light Sci Appl 2015;4(11):1–13. https://doi.org/10.1038/lsa.2015.131.

[17] Eldada, L.; Member, S.; Shacklette, L. W. Advances in polymer integrated optics. 2000, 6 (1), 54–68.

[18] Paquet, C.; Kumacheva, E. Polymers for photonics. 2008, 11 (4), 48–56.

[19] Search, H.; Journals, C.; Contact, A.; Iopscience, M.; Address, I. P. SU-8: a low-cost negative resist For MEMS. 1997, 121–124.

[20] Eryürek M, Tasdemir Z, Karadag Y, Anand S, Kilinc N, Alaca BE, Kiraz A. Integrated humidity sensor based on SU-8 polymer microdisk microresonator. Sensors Actuators, B Chem 2017;242:1115–20. https://doi.org/10.1016/j.snb.2016.09.136.

[21] Zhao Y, Grischkowsky DR. 2-D terahertz metallic photonic crystals in parallel-plate waveguides. IEEE Trans Microw Theory Tech 2007;55(4):656–63. https://doi.org/10.1109/TMTT.2007.892798.

[22] Ji L, Sun X, He G, Liu Y, Wang X, Yi Y, Chen C, Wang F, Zhang D. Surface plasmon resonance refractive index sensor based on ultraviolet bleached polymer waveguide. Sens Actuators B Chem 2017;244:373–9. https://doi.org/10.1016/j.snb.2017.01.006.

[23] Nitiss E, Bundulis A, Tokmakovs A, Busenbergs J, Rutkis M. All-organic waveguide sensor for volatile solvent sensing. Photonic Sens 2019;9(4):356–66. https://doi.org/10.1007/s13320-019-0543-z.

[24] Malinauskas M, Baltriukiene D, Kraniauskas A, Danilevicius P, Jarasiene R, Sirmenis R, Zukauskas A, Balciunas E, Purlys V, Gadonas R, Bukelskiene V, Sirvydis V, Piskarskas A. In vitro and in vivo biocompatibility study on laser 3D microstructurable polymers. Appl Phys A Mater Sci Process 2012;108(3):751–9. https://doi.org/10.1007/s00339-012-6965-8.

[25] Lorang DJ, Tanaka D, Spadaccini CM, Rose KA, Cherepy NJ, Lewis JA. Photocurable liquid core-fugitive shell printing of optical waveguides. Adv. Mater. 2011;23(43):5055–8. https://doi.org/10.1002/adma.201102411.

[26] Girschikofsky M, Rosenberger M, Förthner M, Rommel M, Frey L, Hellmann R. Waveguide bragg gratings in Ormocer®s for temperature sensing. Sensors (Switzerland) 2017;17(11):1–9. https://doi.org/10.3390/s17112459.

[27] Madani A, Azarinia H, Latifi H. Design and fabrication of a polymer micro ring resonator with novel optical material at add/drop geometry using laser beam direct write lithography technique. Optik (Stuttg) 2013;124(14):1746–8. https://doi.org/10.1016/j.ijleo.2012.06.003.

[28] Liang Y, Zhao M, Wu Z, Morthier G. Bimodal waveguide interferometer RI sensor fabricated on low-cost polymer platform. IEEE Photonics J. 2019;11(2):1–8. https://doi.org/10.1109/JPHOT.2019.2900741.

[29] Zhao WM, Wang Q. Analytical solutions to fundamental questions for lossy mode resonance. Laser Photonics Rev 2023;17(1):1–18. https://doi.org/10.1002/lpor.202200554.

[30] Letko E, Bundulis A, Mozolevskis G. Lossy mode resonance sensors based on planar waveguides: theoretical and experimental comparison. IEEE Photonics J 2024;16 (1):1–7. https://doi.org/10.1109/JPHOT.2023.3348993.

[31] The Lorentz Oscillator Model and Beyond *Extrem. Nonlinear Opt.* 2005, 27–59. 10.1007/3-540-26688-7_3.

[32] Woollam J.A., Spectroscopic Ellipsometers C. *CompleteEASE data acquisition and analysis software for software manual*. 2011.

[33] Wei J, Murray JM, Barnes JO, Krein DM, Schunemann PG, Guha S. Temperature dependent sellmeier equation for the refractive index of GaP. In: Proceedings of the Conference Lasers Electro-Optics. 2; 2017. p. 1–3. https://doi.org/10.1364/CLEO_SI.2017.SW4M.3. *CLEO 2017 - Proc. 2017*-Janua.

[34] Prajzler V, Jašek P, Nekvindová P. Inorganic–organic hybrid polymer optical planar waveguides for Micro-Opto-Electro-Mechanical Systems (MOEMS). Microsyst. Technol. 2019;25(6):2249–58. https://doi.org/10.1007/s00542-018-4105-x.

[35] Piruska A, Bhagat AAS, Zhou K, Peterson ETK, Papautsky I, Seliskar CJ. Characterization of SU-8 optical multimode waveguides for integrated optics and sensing on microchip devices. Microfluid. BioMEMS, Med. Microsyst. IV 2006; 6112:1–9. https://doi.org/10.1117/12.655667. 611207.

[36] Kadhim, R. A.; Yuan, L.; Xu, H.; Wu, J.; Member, S.; Wang, Z. Highly sensitive D-shaped optical fibre surface plasmon resonance refractive index sensor based on Ag- α -Fe2O3 grating. 2020, 1748 (c), 1–11. 10.1109/JSEN.2020.2992854.
[37] Zhang Y, Zhang P, Zhao M, Xu D, Wang J, Li Z, Tang T, Shen J, Li C. A high sensitivity lossy mode resonance refractive index sensor based on SBS structure. Results Phys 2022;36(January):1–10. https://doi.org/10.1016/j.rinp.2022.105454. 105454.
[38] Zhao Y, Wu L, Gan S, Ruan B, Zhu J, Dai X, Xiang Y. High figure of merit lossy mode resonance sensor with graphene. Plasmonics 2019;14(4):929–34. https://doi.org/10.1007/s11468-018-0876-2.